IMPLEMENTATION OF VISCOUS EFFECTS IN RELAP5-3D THERMAL HYDRAULICS CODE

Raymond C. Wang

Office of Science, Science Undergraduate Laboratory Internship

Correspondence: raymondchenranwang@berkeley.edu

University of California, Berkeley

Idaho National Laboratory

Idaho Falls, Idaho

August 4, 2009

IMPLEMENTATION OF VISCOUS EFFECTS IN RELAP5-3D THERMAL HYDRAULICS SAFETY CODE

RAYMOND C. WANG AND DR. GEORGE L. MESINA

ABSTRACT

The Reactor Excursion Leak Analysis Program (RELAP5-3D) is a world class thermal hydraulics safety analysis code developed at the Idaho National Laboratory (INL) to address safety concerns in light water nuclear reactors. The purpose of this project is to implement viscous effects into the current RELAP5-3D code. Viscous effects have been thoroughly studied and implemented in many Computational Fluid Dynamics (CFD) codes. However, because of the original purpose of RELAP5-3D, viscous effects on fluid dynamics were not implemented during initial code development. As demand for coupling RELAP5-3D with CFD codes increases, implementing viscous effects in RELAP5-3D is becoming more important both for calculation accuracy and code coupling stability. The momentum flux equations used in RELAP5 resemble the Navier-Stokes Equations (NSE) but doesn't include the viscous contributions. Therefore, a double central finite difference method is used to discretize second order differentials of the viscous terms in both Cartesian and cylindrical geometries. A total of 20 new terms were introduced and the original RELAP5 wall boundary condition was changed from free slip to no slip. The original code architecture was not changed during any of the coding to avoid introducing new limitations. Two test models were used to analyze the performance using water as working fluid. The 3D cylindrical pipe model was used to test if a Poiseuille velocity profile could be generated for laminar flow regimes. The rectangular duct model was used to test for functionality of the viscous terms in Cartesian geometry. A comparison between the calculations from the modified and unmodified RELAP5-3D for the cylindrical pipe was made. The modified calculations converged in approximately 300 seconds to a classic parabolic Poiseuille flow profile with an error from analytical results of 2.28%, whereas the unmodified calculations converged in 600 seconds to a profile with plug flow characteristics. These results demonstrate a significant improvement in both convergence time and accuracy. Thus, implementation of viscous effects in RELAP5-3D is not only achievable, but also beneficial to convergence speed. Further development of the viscous effect can expand capabilities to include modeling turbulent viscous effects, two phase effects, or effects using nearly implicit advancements.

INTRODUCTION

The Reactor Excursion Leak Analysis Program – Three Dimensional (RELAP5 – 3D) is a world class simulation code that was originally developed to assess the safety and reliability of light water nuclear reactor designs under various transients [1]. The code is capable of modeling

effects of thermal hydraulics, heat transfer, and neutron kinetics in large scale systems as well as single hydrodynamic components. Because of the original purpose of the code, most RELAP5-3D thermal hydraulics problems studied are in the turbulent flow regime with small length to diameter (L/D) ratio, such that viscous effects would be negligible. In addition, the original RELAP5 code utilizes 1D momentum flux equations for 1D hydrodynamic components, which are unable to simulate multidimensional terms such as viscous stress tensors. Therefore, viscous effects on momentum flux were not implemented in the original code development. However, implementing these effects would increase stability of multi-code coupling, speed of convergence, and accuracy of results.

A capability to couple RELAP5-3D with other computer programs via Parallel Virtual Machine (PVM) [2] allows both modeling of more complex physical models and more detailed modeling of sub-regions of existing models [3]. Coupling RELAP5-3D with commercial Computational Fluid Dynamics (CFD) codes, such as Fluent [4], to achieve improved accuracy in large flow regions presented a problem with discrepancy between RELAP5 and CFD data. Most commercial CFD codes include viscous effects for both turbulent and laminar flow regimes and are therefore fully capable of generating accurate approximations of experiment results on a localized scale, while RELAP5-3D does not. More accurate coupled calculations with CFD codes could be achieved if viscous effects were incorporated in RELAP5-3D.

With its 3D components, RELAP5-3D has the ability to include multidimensional effects such as viscosity, but because it dealt mostly with overall system responses rather than localized phenomenon, there was little incentive to include these effects until recently. In a comparison

made in 2003, RELAP5-3D was unable to arrive at the same solution as Fluent or experiment

data because it not only lacks viscous stress effects, but also imposes a "free-slip" wall boundary

condition [5]. Therefore, in a cylindrical pipe with turbulent or laminar flow regime, RELAP5

would produce a uniform velocity profile from wall to wall, where as, commercial CFD codes

with "no-slip" boundary conditions and viscous effects would typically arrive at plug velocity

profile for turbulent regimes and an approximate Poiseuille velocity profile for laminar regimes.

The equations governing RELAP5-3D calculations of momentum flux in a 1D region are

expressed as the following [1]:

$$
\alpha_f \varrho_f A \frac{\partial v_f}{\partial t} + \frac{1}{2} \alpha_f \varrho_f A \frac{\partial v_f^2}{\partial z} =
$$

$$
-\alpha_f A \frac{\partial P}{\partial z} + \alpha_f \varrho_f B_x A - (\alpha_f \varrho_f A) FWF(v_f) - \Gamma_g A(v_{fI} - v_f)
$$

$$
-(\alpha_f \varrho_f A) FIF(v_f - v_g) - C\alpha_f \alpha_g \varrho_m A[\frac{\partial (v_f - v_g)}{\partial t} + v_g \frac{\partial v_f}{\partial z} - v_f \frac{v_g}{\partial z}]
$$

(1)

$$
\alpha_g \varrho_g A \frac{\partial v_g}{\partial t} + \frac{1}{2} \alpha_f \varrho_g A \frac{\partial v_g^2}{\partial z} =
$$

$$
-\alpha_g A \frac{\partial P}{\partial z} + \alpha_g \varrho_g B_x A - (\alpha_g \varrho_g A) FWG(v_g) + \Gamma_g A(v_{gI} - v_g)
$$

$$
-(\alpha_g \varrho_g A) FIG(v_g - v_f) - C\alpha_f \alpha_g \varrho_m A[\frac{\partial (v_g - v_f)}{\partial t} + v_f \frac{\partial v_g}{\partial z} - v_g \frac{\partial v_f}{\partial z}]
$$

(2)

While these equations are two phase and can take into consideration the effects of interface

friction, wall friction, as well as mass transport between the two phases, they are limited to

inviscid 1D calculation. The scheme used to discretize these equations is a Bernoulli corrected upwind difference scheme for both semi-implicit and nearly implicit schemes [6]. Further improvements were made with the introduction of LeVeque type method into 3D components. These equations are then applied to 3D hydrodynamic components such that each geometric component is solved separately with first order accuracy.

The objective of this project is to implement viscous stress tensors into the current RELAP5-3D momentum flux equations without modifying the main code architecture. The range of implementation is limited to only laminar flow regimes in cylindrical pipes and rectangular ducts. The implementation is further limited to modeling only liquid phase incompressible fluids and only the semi-implicit time advancement technique.

There are two major complications involved in implementing the stress tensors. Firstly, each of the second order partial differential stress terms must be discretized using a finite difference scheme across meshing that could be perpendicular or parallel to the direction of the velocity vector. Secondly, the code's 3D discretization uses a "free-slip" wall boundary condition rather than the "no-slip" condition needed for Poiseuille flow. The methods used to address these complications will be discussed in the Materials and Methods section.

MATERIALS AND METHODS

Momentum Equations

The fundamental effects governing analytical behaviors of momentum flux in Cartesian, cylindrical, and spherical geometries are given by the Navier-Stokes Equations (NSE). The cylindrical geometry, single phase, constant coefficient of viscosity, and constant density form of the Navier-Stokes Equations is expanded as the following [7]:

$$
\rho\left(\frac{\partial v_r}{\partial t} + v_r\frac{\partial v_r}{\partial r} + \frac{v_\theta}{r}\frac{\partial v_r}{\partial \theta} - \frac{v_\theta^2}{r} + v_z\frac{\partial v_r}{\partial z}\right) =
$$
$$
-\frac{\partial p}{\partial r} + \rho g_r + \mu\left[\frac{\partial}{\partial r}\left(\frac{1}{r}\frac{\partial}{\partial r}(rv_r)\right) + \frac{1}{r^2}\frac{\partial^2 v_r}{\partial \theta^2} - \frac{2}{r^2}\frac{\partial v_\theta}{\partial \theta} + \frac{\partial^2 v_r}{\partial z^2}\right]
$$
(3)

$$
\rho\left(\frac{\partial v_\theta}{\partial t} + v_r\frac{\partial v_\theta}{\partial r} + \frac{v_\theta}{r}\frac{\partial v_\theta}{\partial \theta} + \frac{v_r v_\theta}{r} + v_z\frac{\partial v_\theta}{\partial z}\right) =
$$
$$
-\frac{1}{r}\frac{\partial p}{\partial \theta} + pg_\theta + \mu\left[\frac{\partial}{\partial r}\left(\frac{1}{r}\frac{\partial}{\partial r}(rv_\theta)\right) + \frac{1}{r^2}\frac{\partial^2 v_\theta}{\partial \theta^2} + \frac{2}{r^2}\frac{\partial v_r}{\partial \theta} + \frac{\partial^2 v_\theta}{\partial z^2}\right]
$$
(4)

$$
\rho\left(\frac{\partial v_z}{\partial t} + v_r\frac{\partial v_z}{\partial r} + \frac{v_\theta}{r}\frac{\partial v_z}{\partial \theta} + v_z\frac{\partial v_z}{\partial z}\right) =
$$
$$
-\frac{\partial p}{\partial z} + \rho g_z + \mu\left[\frac{1}{r}\frac{\partial}{\partial r}(r\frac{\partial v_z}{\partial r}) + \frac{1}{r^2}\frac{\partial^2 v_z}{\partial \theta^2} + \frac{\partial^2 v_z}{\partial z^2}\right]
$$
(5)

The Cartesian geometry viscous terms of the NSE has some differences, but are simpler than these cylindrical ones. Both the cylindrical and the Cartesian geometry viscous stress tensors were implemented, and their discretization schemes are similar.

Discretizing Viscous Terms

The viscous stress tensors in 3D NSE require discretizations across meshes that are often not in the same direction as the velocity vector. In addition, because most of the viscous terms are second order partial differentials, the finite differencing scheme has to properly discretize the values of each term twice with first order accuracy. Instead of a Bernoulli corrected upwinding method or a Leveque method, a double central differencing method was chosen to discretize each of the viscous terms. This method requires data from at least three momentum volumes to generate one finite difference approximation to one viscous term. An example of this scheme used on one of the viscosity terms is shown in Equation 6. Equation 6 is the double central finite difference scheme for the viscous momentum flux contribution of the liquid velocity in the axial direction, changing with respect to the radial direction. Where Δr_i is the radius difference at volume i,j,k, r_i, $r_{i+1/2}$ and $r_{i-1/2}$ are the values of radius for control volume i,j,k at its center, top, and bottom respectively, and $v_{z,i+1}$, $v_{z,i-1}$ and $v_{z,i}$ are the axial velocities at locations i+1,j,k+1/2, i-1,j,k+1/2, and i,j,k+1/2 respectively. See Figure 1.

$$\frac{1}{r}\frac{\partial}{\partial r}\left(r\frac{\partial v_z}{\partial r}\right) = \frac{1}{r_i}\left[\frac{r\frac{\partial v_z}{\partial r}\big|_{i+\frac{1}{2}} - r\frac{\partial v_z}{\partial r}\big|_{i-\frac{1}{2}}}{\triangle r_i}\right]$$

$$= \frac{1}{r_i}\left[\frac{r_{i+\frac{1}{2}}\left[\frac{v_{z,i+1}-v_{z,i}}{\frac{1}{2}(\triangle r_{i+1}+\triangle r_i)}\right] - r_{i-\frac{1}{2}}\left[\frac{v_{z,i}-v_{z,i-1}}{\frac{1}{2}(\triangle r_i+\triangle r_{i-1})}\right]}{\triangle r_i}\right]$$

(6)

This expression calculates the viscous effects of momentum flux at momentum cell i,j,k+1/2, using data from cells i+1,j,k+1/2, i-1,j,k+1/2, and i,j,k+1/2 taken from the previous semi-implicit time step. The implementation also included considerations for negative velocity profiles.
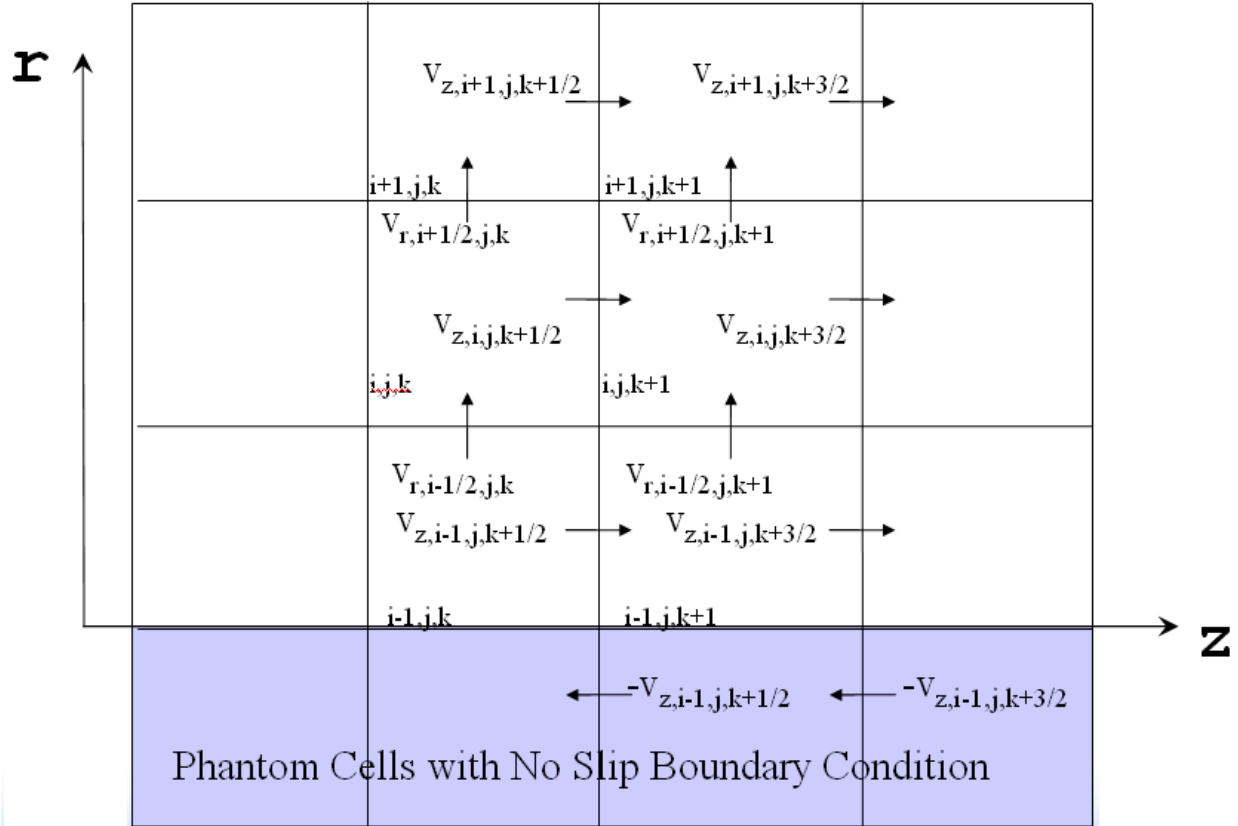
Figure 1: R-Z coordinate grid map of momentum cell discretization scheme.

Using the velocities shown in Figure 1, Equation 6 first finds the central difference of $V_{z,i+1,j,k+1/2}$ and $V_{z,i,j,k+1/2}$, then $V_{z,i-1,j,k+1/2}$ and $V_{z,i,j,k+1/2}$. It then utilizes these two differences to find a third central difference, which derives the desired solution. .

Setting Wall Boundary Conditions

The wall boundary condition is set to no slip through setting all phantom cells (cells not in the flow region, but which represent the boundary) of physical walls to have the same magnitude but opposite direction as those of the adjacent control volume. This way, the average velocity on the wall between the volume and the phantom cell is effectively zero. If the wall boundary condition

is left as the default free slip condition, the velocity vector inside the phantom cell would then be the same as that in the previous volume, thus the average, i.e. velocity at the inner wall, would be nonzero. However, the free slip condition does not generate Poiseuille flow profiles because the analytical Poiseuille wall boundary condition is a no slip condition.

Test Cases

Two Poiseuille flow test models were created to test the accuracy of the modified RELAP5-3D coding and for comparison with the unmodified code. The first model is pictured in Figure 2.
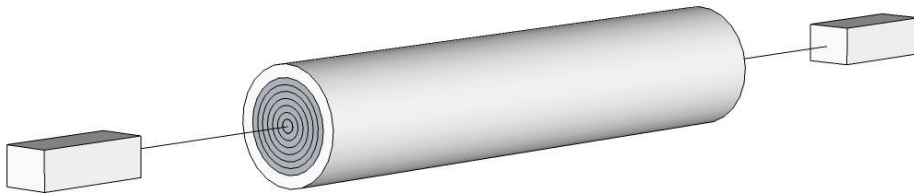

Figure 2: 3D representation of the Cylindrical Test Model. (Not to Scale)

The first model is a 3D cylindrical pipe with 25 axial zones each 100.0 m long and nine radial zones with a total diameter of 2 m. It is based on the one used in the 2003 comparison study [5].

Smaller versions of the cylindrical pipe were also tested and the results were consistent with those to the large model given scaling considerations

The second model, shown in Figure 3, tests performance of viscous effects in Cartesian geometry. The model has a 5 by 5 by 5 mesh of a rectangular duct with an area of 25 m^2 and a total length of 500 m. This model was created specifically for the purpose of this test, but is also highly adjustable if different dimensions and meshing are needed.
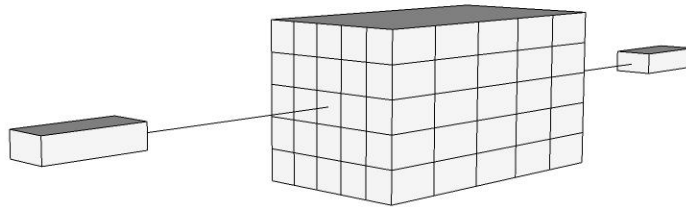
Figure 3: 3D representation of the Cartesian Test Model (Not to Scale)

.

Analytical Results and Calculations

The Poiseuille flow formulation given below can find the velocity of incompressible fluids at any point in the radial direction under steady state conditions.

$$v(r) = \frac{(p_o - p_L)R^2}{4\mu L}\left[1 - \left(\frac{r}{R}\right)^2\right]$$

(7)

where the variables are summarized in the nomenclature section. In order to derive a form of the equation that relies on easily controllable average velocity inputs rather than pressure differences across the pipe, several simplifications were made. Firstly, using the head loss across the pipe as the change in pressure we find:

$$\Delta p = \frac{64}{Re}\frac{L}{D}\frac{\rho v^2}{2}$$

(8)

Secondly, since the Reynolds Number is given by,

$$Re = \frac{\rho v D_H}{\mu}$$

(9)

Combining Equations 7, 8, and 9 we will derive an equation of the velocity at any point along the radius of a cylindrical pipe as a function of the average steady state velocity:

$$v(r) = \frac{8R^2 \bar{v}}{D_H D}\left[1 - \left(\frac{r}{R}\right)^2\right]$$

(10)

This equation may appear to be independent of viscosity, but in actuality the viscous effects will influence the value of the average velocity. The reason is that this average is found using the Reynolds Number from Equation 9, which determines if a fluid is in a laminar flow regime. In order to find the average of any analytical velocity in any control volume at r_i, the following integration is needed:

$$\bar{v}(r_i) = \frac{\displaystyle\int_{r_{i-1/2}}^{r_{i+1/2}} v(r)\,dr}{\displaystyle\int_{r_{i-1/2}}^{r_{i+1/2}} dr} \tag{11}$$

Convergence in Space

The inlet conditions for the two models were either a flat velocity profile of the average axial velocity or a fully developed analytical Poiseuille flow. Both the steady and unsteady profiles are allowed to fully develop before being analyzed at the entry junction of the last axial zone. Analysis at the entrance as well as along the pipe before the flow is fully developed is also possible for shorter models, but because the purpose was not to analyze entrance effects these were not collected.

Convergence in Time

The initial conditions for both tests were set such that no fluid was moving at time equal zero seconds. For the pipe model, two simulations of different time durations were made for each inlet boundary condition of both modified and unmodified. The first simulations were run to 100.0 seconds simulation time, not Central Processing Unit (CPU) time, when the velocity profiles as well as magnitudes have yet to converge to analytical solutions due to the unsteady nature of the model with its stagnant initial condition as well as RELAP5's transient simulation capabilities. The second set of simulations was run for 1000.0 seconds when the velocity profiles and magnitudes have fully converged upon various steady state solutions. These sets are used to quantitatively evaluate the performance improvements or deteriorations of the modified over that of the unmodified RELAP5-3D.

Error with Increasing Reynolds Number

Another study was to calculate the error of results from the modified RELAP5-3D compared to those of the analytical results for Poiseuille flow in the cylindrical model. Only the analytical average velocity of the center most control volume was compared to those from the RELAP5 results, because the center-most control volume appeared to have the highest percentage of error. This analysis was done at a range of Reynolds Numbers from 50 to 2000. The Reynolds Number was varied through adjusting the flow rates of the inlet plug flow velocity profile as show in Equation 9. The error was then plotted as a function of Re. This can be seen in Figure 6.

Working Fluids

The working fluid used for these tests was incompressible water. However, other fluids available to RELAP5-3D such as molten salt can also be used to test the functionality of the modified RELAP5-3D. As long as the models are corrected for changes in fluid properties, the laminar Poiseuille profile does not change because the implementation of the viscous terms is not fluid specific. The assumption of incompressibility comes from the simplicity of the equations used to both implement the viscous terms and to produce the analytical solutions.

RESULTS AND DISCUSSION

The results from the cylindrical models vary with respect to both transient time and modification, but not initial velocity profile type. The results shown in Figure 4 are taken from the last of the inlet junction of the 25th axial volume across from the inner most radial control volume to the outer most control volume. All data are plotted as average velocity, in meters per second, of a control volume versus distance between the center of the pipe and the center of the control volume in meters. Therefore, the last control volume is at radius equals 0.94 meters rather than at radius equals 1.0 meter, which is at the inner wall.
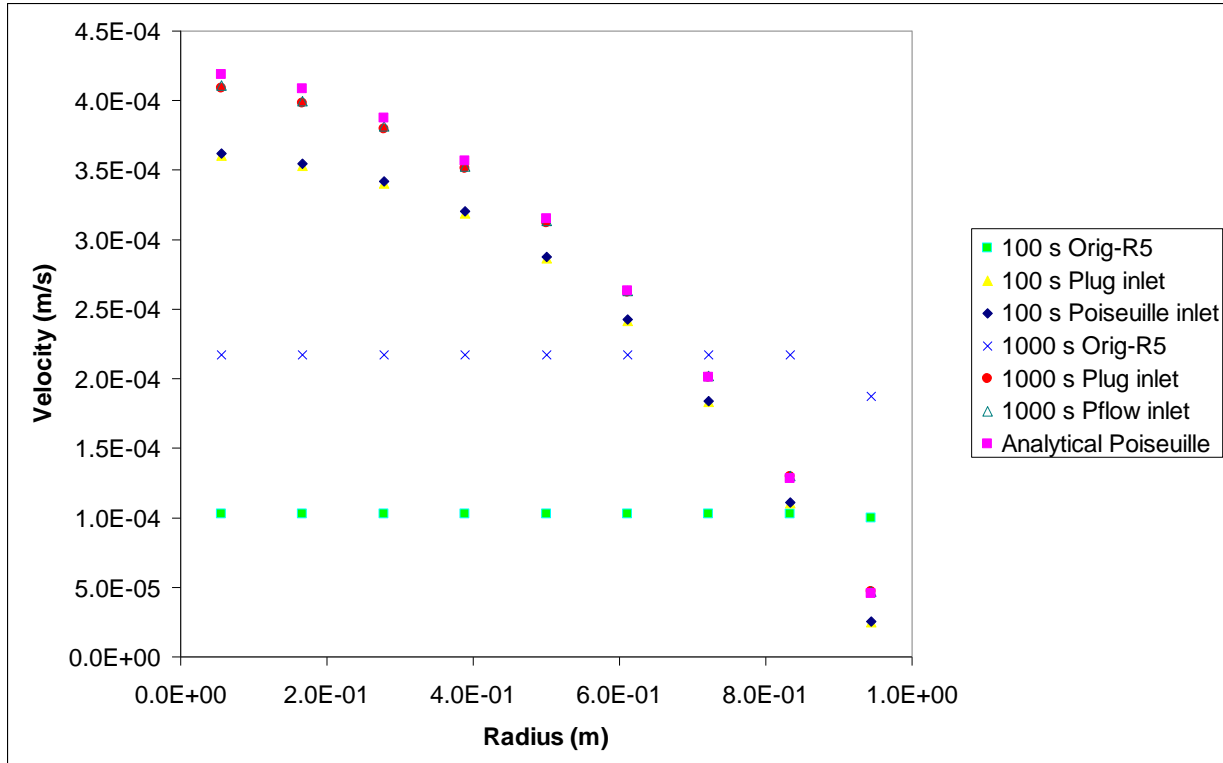
Figure 4: Plot of Velocity profile as a function of Radius of Cylindrical Test Model Results

Each of the different types of plotted symbols represents the results from one run. The green square is a 100.0 second simulation run that uses the unmodified RELAP5-3D code. It has a very flat profile and is at a magnitude that is half of the inlet velocity's magnitude. The yellow diamond series represents a 100.0 second simulation run that uses the modified RELAP5-3D code and has a plug inlet profile. This series overlaps a similar series marked as blue diamonds, which has similar characteristics except its inlet condition had an analytical Poiseuille profile. These two series have a parabolic profile, but still have a large difference from the analytical results. The blue x series is the same as the green squares except the simulation was run for 1000.0 seconds. It also has a very flat profile but does exhibits a sharp drop near the wall of the pipe. The series marked as red circles and blue triangles are similar to the yellow diamond and blue diamonds series respectively. However, these two new series were allowed to run for

1000.0 seconds and are much closer to the analytical Poiseuille profile in both magnitude and curvature. Finally, the analytical calculation of the Poiseuille flow is given in the pink square series. These values were not calculated by RELAP5 but rather generated using the Equation 11.

The first observation is that initial and inlet boundary conditions have very little affect on the solution as any differences seem to have quickly collapsed before 100.0 seconds of simulation. Secondly, the difference between the 1000.0 seconds runs of modified and unmodified RELAP5-3D is very significant. The original RELAP calculated a profile roughly resembling those of turbulent profiles which as shown in Nikuradse's data are not even flat [9]. In stark contrast, the modified RELAP calculated profiles had multiple points where the analytical and the simulated results overlapped, and those points not overlapping were very close to each other when compared to results of the unmodified calculations. The 100.0 second runs were all less accurate in magnitude and curvature. However, the parabolic shape of Poiseuille profile is still recognizable in the 100.0 seconds runs of the modified RELAP5, where as the original calculations fell short of having the correct magnitude and forming any recognizable curvature.

The next set of results collected was for an analysis of the effects on convergence from the viscous contributions. In the following figure, a plot of the solution RELAP5 calculates for the volume average velocity at the outermost radial zone in the last axial zone as simulation time advances. As time advances with the semi-implicit method, initial instabilities damp out and the solution converges after a certain amount of time, to Poiseuille profile for various velocity profiles and inlet boundary conditions.
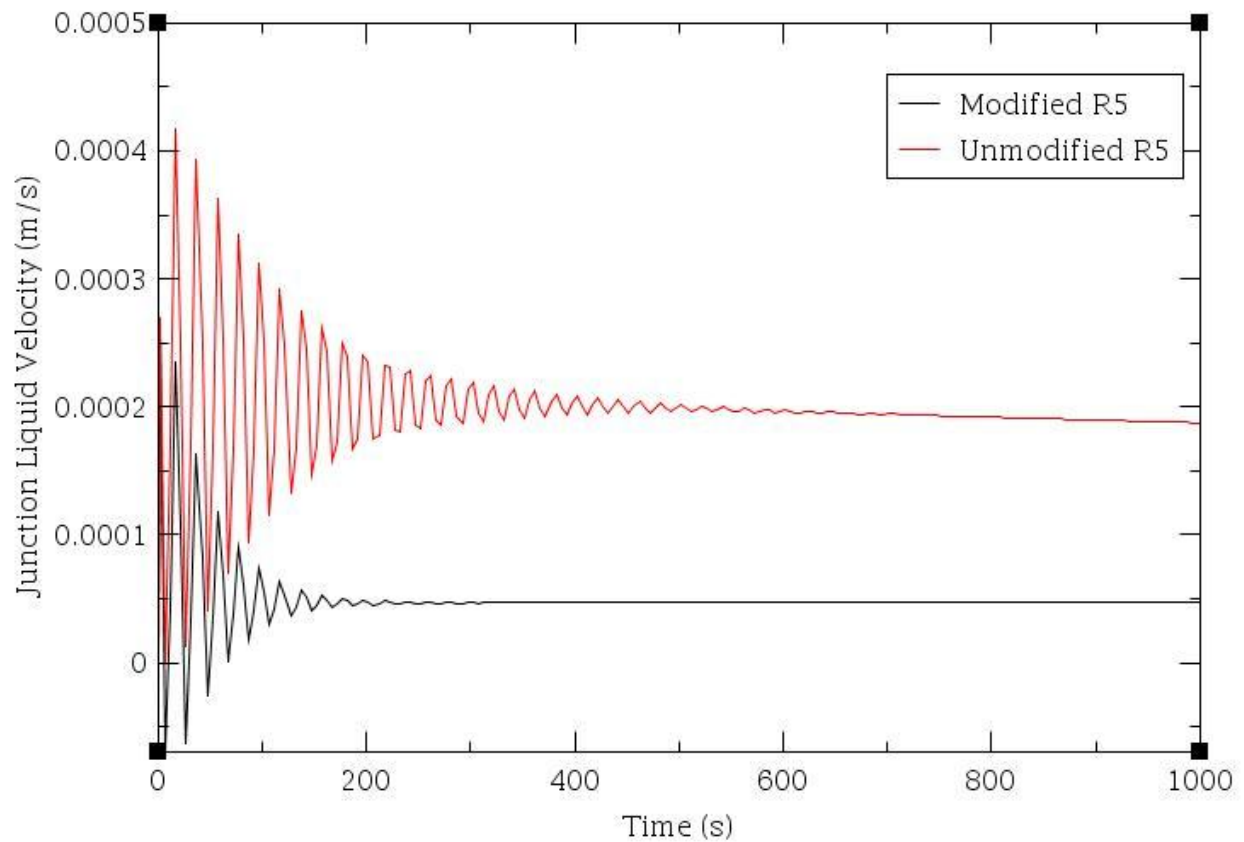
Figure 5: Plot of Convergence of Solution in time.

The two simulations converged at different times even though they had the same inlet and initial

conditions. The modified RELAP5 calculations shown in black converged to a steady solution at

approximately 300 seconds after initialization. However, the unmodified RELAP5 calculations

took approximately 600 seconds if not more. In addition, the two calculations converged at two

different velocities. The unmodified RELAP5 arrived at an incorrect value of approximately

1.8×10^{-4} m/s, while the modified code correctly calculated the velocity to be approximately

4.5×10^{-5} m/s. In fluids more viscous than water, the damping effects of the viscosity terms will

become even more apparent, such that the modified RELAP5-3D will not produce an oscillating initial transient.

A third analysis of the cylindrical model was made to determine the contribution of error as inlet fluid flow rate is changed in magnitude. The error is found through the difference between calculated results from the 1000.0 seconds run and the analytical results. The error of the RELAP5 results versus Reynolds Number is plotted below.
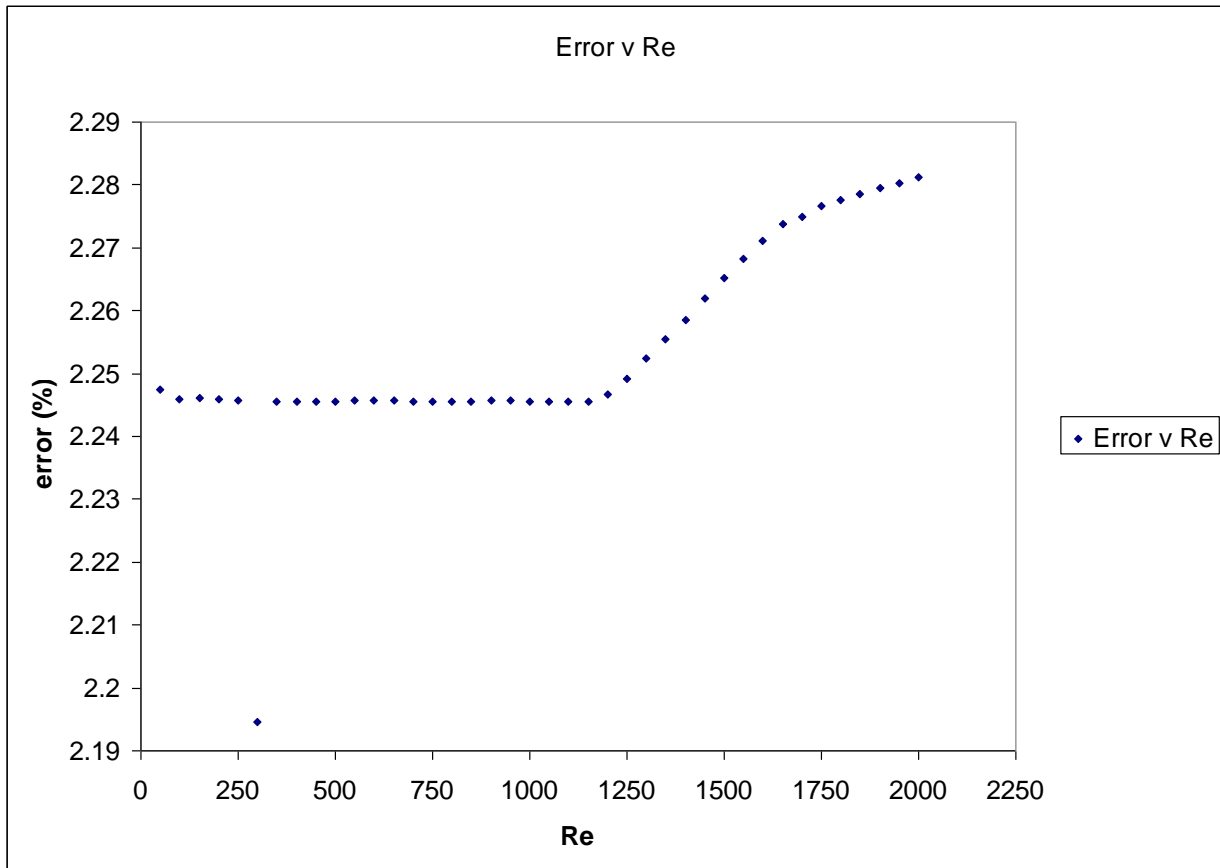

Figure 6: A plot of dimensionless error versus dimensionless Reynolds Number

The results show that at lower Reynolds Numbers the error of the calculations was relatively constant, but as the Reynolds Number passes 1200 the error begins to increase. There is one

outlier at Re equals 300 that is approximately 2.19 percent. However, the difference is actually less than 0.05 of a percent, 0.0005, from the average values with Re ranging from 50 to 1200. The increase in error after Re 1200 is most likely due to the transition between laminar and turbulent regimes. The analytical Poiseuille profile is only valid in the laminar regime, and as RELAP5 begins to introduce its original turbulence effects for 1D inviscid flow the accuracy of its calculations compared to those of idealistic laminar flow is reduced. Until turbulence viscous effects are implemented, turbulent flow velocities should be avoided.

The Cartesian model results were analyzed using a more qualitative standard due to the lack of comparison to analytical results. However it was expected that the flow profile should resemble the parabolic profile similar to those in cylindrical Poiseuille flow [8]. A three dimensional representation of the axial velocity vector at a cross section of the inlet junction into the last axial zone is generated below. See Figure 7.

Again, these velocities are averages for the entire control volume that they originate. The overall shape of the vector field is a parabolic surface. This result didn't change even when the inlet condition was changed. The 2D cross sections of this 3D vector field also generate parabolic curves, as shown in Figure 8, of the diagonal cross section along the x-y plane.

In original RELAP5 calculations, the velocity profiles would remain flat. The parabolic profiles formed in these rectangular ducts are due to the no slip wall conditions as well as the viscous effects. The viscous effects in this case travel in both x and y directions as well as affect the calculations of the next axial control volume layer. The result is the formation of a parabolic

surface, that if reduced to a two dimensional curve, would produce a parabolic curve along any

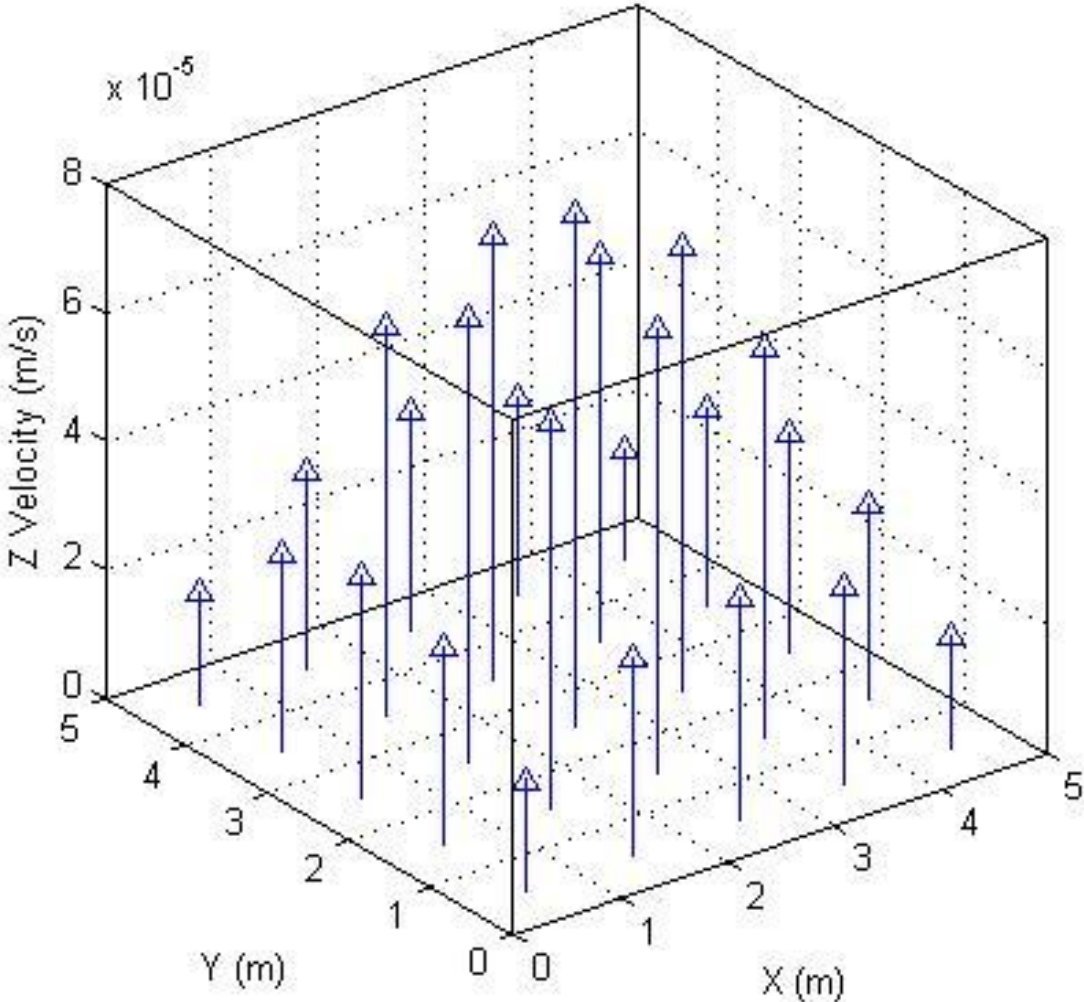set of points parallel to the x axis, y axis, or x-y diagonals.

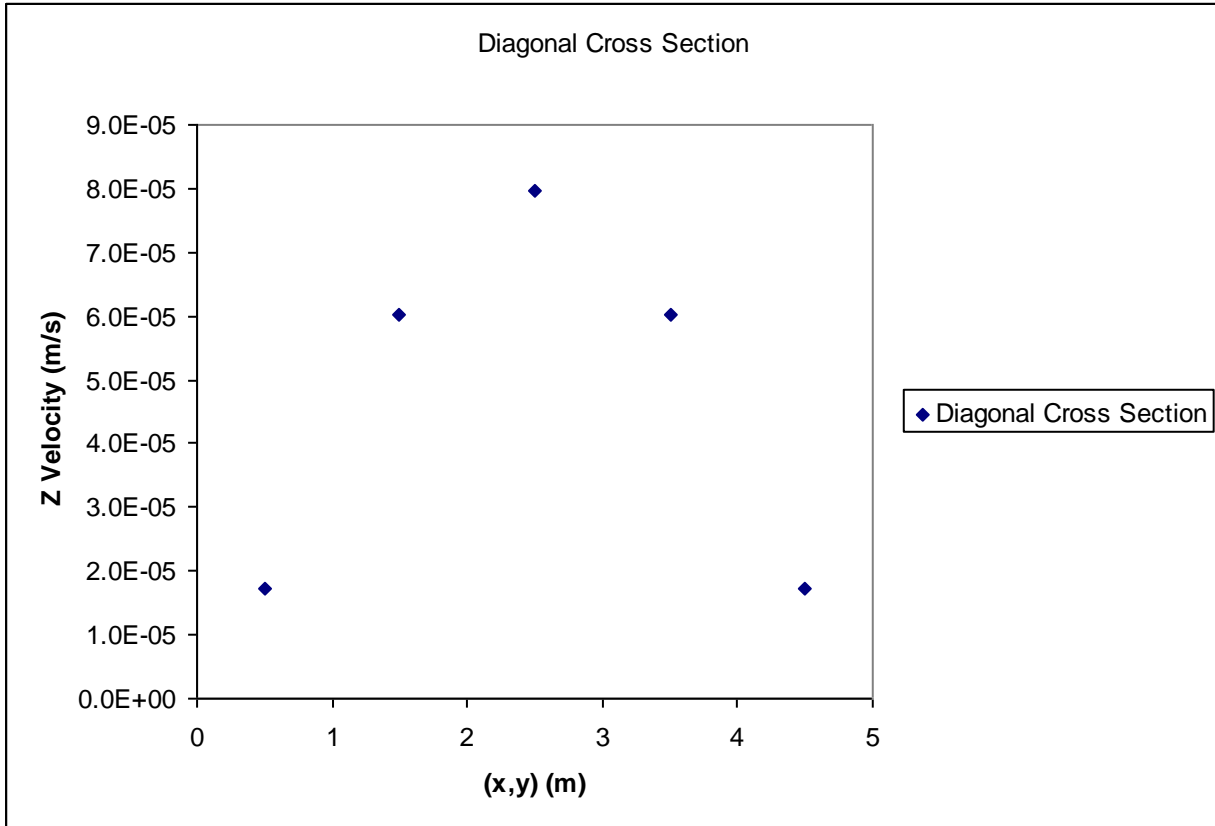**Figure 7:** 3D representation of axial velocity vectors on the x-y plane of a cross section.

Figure 8: 2D diagonal cross section of the axial velocity profile inside a rectangular duct.

CONCLUSIONS

From the results of the simulations, the viscous modified RELAP5-3D is very attractive from the standpoint of both accuracy and efficiency. As shown in Figure 4, the calculated results from modified RELAP5-3D closely matched those of the analytical Poiseuille flow. In contrast, the calculations from the original RELAP5-3D code produced flat profiles, which matched more closely with turbulent flow profiles than laminar ones. This difference of results comes from the new "no-slip" boundary conditions which are able to create slow flow rates at the outermost

control volume. Then the 3D viscous terms help transfer these wall effects across the entirety of the pipe through the multidimensional discretization scheme as exemplified in Equation 6.

In addition, the modified RELAP5 is capable of converging at this accurate laminar solution after only half of the time it takes for the unmodified code to arrive at an inaccurate solution as show in Figure 5. This clearly demonstrates the improvement in efficiency provided by the viscous effects. Furthermore, because the original code converged upon the wrong velocity, it may continue to remain semi-stable. Compared to the results comparison shown in the previous study, the relative differences between RELAP5 calculations and analytical results have been greatly reduced [5]. However, the 2003 study was on turbulent flow regimes. The error between the Nikuradse results and the modified RELAP5 calculations is predictably large as shown in Figure 6, because the turbulence viscous models are yet to be implemented.

There are still several limitations to the viscous code. The implemented viscous effects are currently limited to modeling liquid, laminar, fully developed flows. However, the original RELAP5 can model two phase, turbulent or laminar, transient flows; thus, have the capacity to enter into regimes outside of the modified limitations. In order to retain the capabilities and robustness of the original RELAP5, the viscous effects implemented will become an optional feature that can be added or removed without reinstalling the RELAP5-3D program. Further development of viscous effects will eventually include turbulence regime effects, two phase viscous equations, and entrance-exit effects. After verification and validation of these implementations, the fully developed viscous effects will enter the main code architecture as a standard contributor rather than an optional one.

ACKNOWLEDGEMENTS

NOMENCLATURE

A	Area
α_f	Liquid void fraction
α_g	Vapor void fraction
B_x	Body force in x coordinate
C	Coefficient of virtual mass
D	Diameter of pipe
D_H	Hydraulic diameter of pipe
FIF	Interface drag coefficient fluid
FIG	Interface drag coefficient vapor
FWF	Wall drag coefficient fluid
FWG	Wall drag coefficient vapor
g_r	Gravitational constant in r coordinate
g_θ	Gravitational constant in theta coordinate
g_z	Gravitational constant in z coordinate
Γ_f	Fluid volumetric mass exchange rate
Γ_g	Vapor volumetric mass exchange rate

L	Length of pipe
μ	Viscosity coefficient
P	Pressure
p_o	Inlet Pressure
p_L	Outlet Pressure
ϱ_f	Liquid density
ϱ_g	Vapor density
ϱ_m	Virtual density
v_f	Liquid velocity
v_g	Vapor velocity
v_{fI}	Liquid interphase velocity
v_{gI}	Vapor interphase velocity

REFERENCE

[1]   RELAP5-3D Code Development Team, "Volume I: Code Structure, System Models, and Solution Methods," *RELAP5-3D Code Manual,* June, 2005.

[2]   A. Geist, et al, "PVM 3 user's guide and reference manual," *Tech. Rep. ORNL/TM-12187*, Oak Ridge National Laboratory, May, 1993.

[3]   W. L. Weaver, E. T. Tomlinson, D. L. Aumiller, "A Generic Semi-Implicit Coupling Methodology for Use in RELAP5-3D," *Nuclear Engineering and Design*, vol 211, pp 13-26, 2003.

[4]   Fluent Inc, "Volume 1", *Fluent 5 User Guide*, 1998.

[5]   R. R. Schultz, R. A. Riemke, C.B. Davis, "Comparison: RELAP5-3D Systems Analysis Code & Fluent CFD Code Momentum Eq. Formulations," *RELAP5 User's Group,* August 27th, 2003.

[6]   A. Shieh, K. Carlson, "Software Design and Implementation for the Bernoulli Corrected Upwinding Differencing Scheme for 3D Components," *INEEL Internal Software Report,* pp. 3, August, 1998.

[7]   R.B. Bird, W. E. Stewart, E. N. Lightfoot, "The Equation of Change for Isothermal

Systems," in *Transport Phenomena,* 1st ed. New York: John Wily & Sons, 1960, ch. 3, pp.

85.

[8]   R. B. Bird, W. E. Stewart, E. N. Lightfoot, "Velocity Distribution in Laminar Flow," in

Transport Phenomena, 1st ed. New York: John Wily & Sons, 1960, ch. 2, pp. 62.

[9]   J. Nikuradse, "Laws of Turbulent Flow in Smooth Pipes," *Forschungsheft 356 Supplement

to Engineering Research,* vol 3, B ed., pp. 27, October, 1932.